The Mantle Transition Zone Hosts the Missing HIMU Reservoir Beneath Eastern China

Sheng-Ping Qian[1,2], Alexander R. L. Nichols[3] , Le Zhang[1,4] , Yi-Gang Xu[1,4] , Jie Li[1,4], Yu-Long Guo[2], and Zhong-Yuan Ren[1,4]

[1]State Key Laboratory of Isotope Geochemistry, Guangzhou Institute of Geochemistry, Chinese Academy of Sciences, Guangzhou, China, [2]State Key Laboratory of Marine Geology, Tongji University, Shanghai, China, [3]Department of Geological Sciences, University of Canterbury, Christchurch, New Zealand, [4]Institutions of Earth Science, Chinese Academy of Sciences, Beijing, China

Abstract The Earth's mantle shows large-scale geochemical heterogeneities bounded by several identifiable end-member compositions. However, the origin of extreme mantle reservoirs, for example, high $^{238}U/^{204}Pb$ (HIMU), and their location in the Earth's interior remains poorly constrained. Clinopyroxenes from late Cenozoic Wudi lavas in eastern China have heterogeneous Pb isotopic compositions, even though the erupted lavas are isotopically homogeneous. Our new results provide, to our knowledge, the first evidence for the existence of a HIMU-like component in the sources of late Cenozoic lavas. Analyses of olivines and their host lavas indicate that the basaltic melts are derived from partial melting of carbonated peridotite. The HIMU source is likely to be younger than 700 Ma old and related to subduction events of the Paleo-Asian ocean. In addition to deep and ancient recycling, storage of a metasomatically produced mantle reservoir in the mantle transition zone may be an important mechanism for developing extreme isotopic signatures.

1. Introduction

Extensive geochemical studies of oceanic basalts identify a multitude of mantle compositions that are often roughly grouped into four distinctive geochemical components: Enriched Mantle 1 (EM1), Enriched Mantle 2 (EM2), high-μ (high $^{238}U/^{204}Pb$, HIMU), and a depleted mid-ocean ridge basalt mantle (Zindler & Hart, 1986). The extreme isotopic composition of mantle domains usually records time-integrated recycling processes and the history of continental and oceanic lithosphere (Hanyu et al., 2014; Lassiter & Hauri, 1998; Zindler & Hart, 1986). Determining the processes by which these geochemically heterogeneous mantle reservoirs formed and the timing of their formation will enable a reconstruction of the recycling process and the deep structure of the mantle, ultimately providing a window onto the long-term evolution of the Earth's mantle.

The HIMU (high time-integrated $^{238}U/^{204}Pb$ or high-μ) mantle reservoir is characterized by highly radiogenic Pb ratios ($^{206}Pb/^{204}Pb$ > 20.5) (Zindler & Hart, 1986). Globally, the HIMU lavas are rare in oceanic and continental settings, such as St. Helena and Cook-Austral Islands, and Zealandia, and thus, HIMU is believed to be rare in the mantle (e.g., McCoy-West et al., 2016; Stracke et al., 2003; Zindler & Hart, 1986). The HIMU lavas are usually thought to result from long-term isolation of recycled material with elevated $^{238}U/^{204}Pb$ (μ) ratios at the core-mantle boundary (Castillo, 2015; Hanyu et al., 2014; McCoy-West et al., 2016; Zindler & Hart, 1986). Alternatively, it has been suggested that the HIMU lavas are not deep rooted and are instead likely derived from shallower poorly mixed mantle reservoirs (e.g., the mantle transition zone, MTZ) (Mazza et al., 2019; Scott et al., 2016). Hence, the location, distribution, and formation mechanism of the HIMU reservoir in the mantle are not well constrained.

Here, we report the first in situ analyses of Pb isotopes in pyroxene crystals and the groundmass from the Wudi volcanic rocks in eastern China. Our new geochemical data are combined with existing geophysical, petrological, and geochemical data to speculate on the location and nature of the HIMU reservoir in the mantle. Finally, we assess the possible mechanism responsible for the generation of the highly heterogeneous mantle.
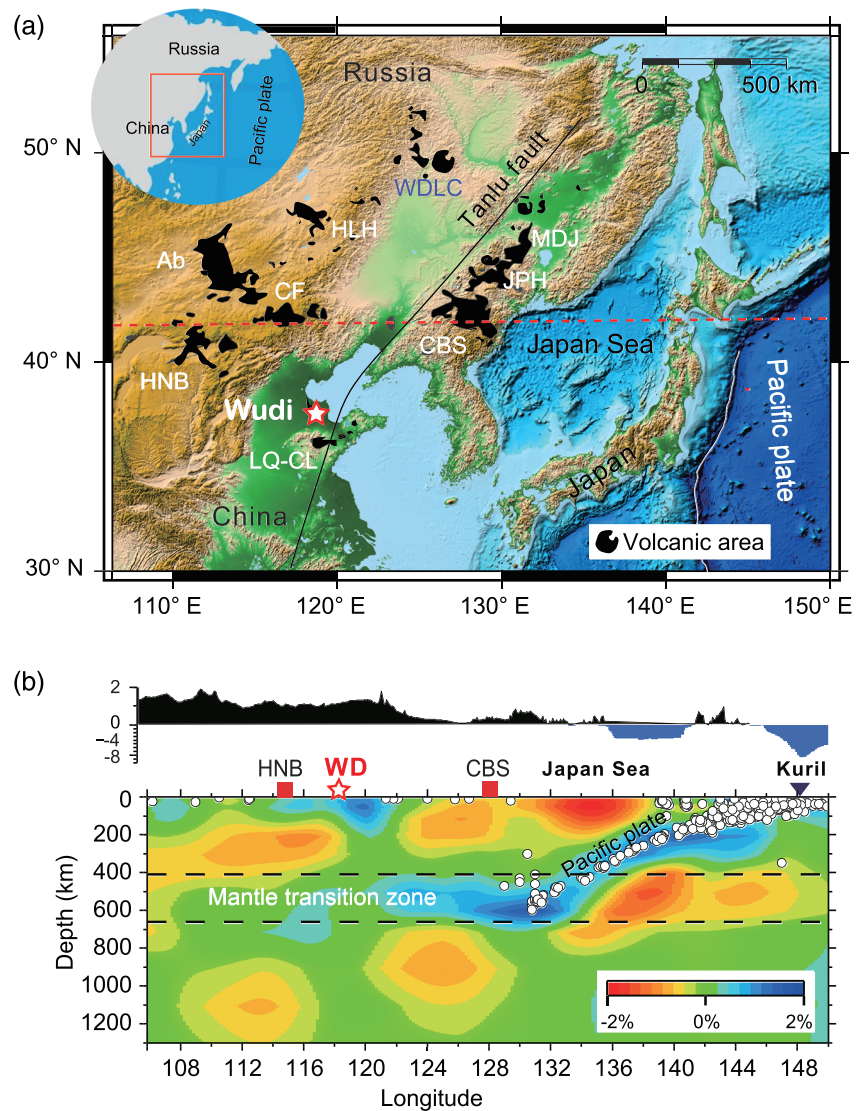
Figure 1. (a) Simplified map of the Cenozoic volcanic province, outcrops denoted by gray fields, in eastern China (modified after Wang et al., 2015). Stars denote sampling locality (Wudi). Acronyms are for volcanic fields and regions: Ch, Changbaishan; CF, Chifeng; Ab, Abaga; HLH, Halaha; HNB, Hannuoba; JPH, Jingpohu; MDJ, Mudanjiang; LQ-CL, Linqu-changle; WDLC, Wudalianchi. (b) Cross section of the mantle seismic tomography at 43°N (red dashed line in (a)) showing the inferred stagnant Pacific slab within the mantle transition zone (defined by the black dashed lines) (Huang & Zhao, 2006). Surface topography along the cross section is shown across the top.

2. Geological Setting and Samples

Eastern China including North China, northeast (NE) China, and surrounding areas lies at the continental margin of the northwest Pacific subduction zone (Figure 1). Late Cenozoic (<23 Ma, since the Miocene) lavas, in particular, are widespread but generally small in volume across eastern China (Figure 1). The duration of magmatic activity in each volcanic field varies greatly, with most of large volcanic fields lasting over tens of million years (Miocene to Pliocene) and some small ones only active for less than 1 Myr. Regardless of spatial and temporal differences, the geochemical compositions of late Cenozoic lavas in eastern China remain largely similar (Chen et al., 2009, 2017; Kimura et al., 2018; Kuritani et al., 2011; Sakuyama et al., 2013; Tang et al., 2006; Zhang et al., 2017). Except for some K-rich rocks in NE China (e.g., Wudalianchi volcanic field), late Cenozoic lavas are generally Na-rich and show a large-scale low $\delta^{26}Mg$ anomaly (Li et al., 2017). The Wudi volcanic field, located in the southeastern part of the North China
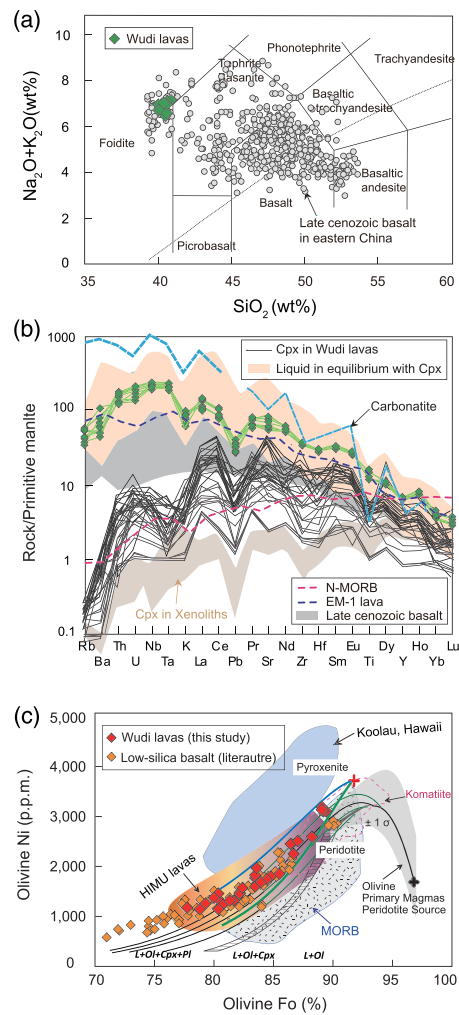
Figure 2. (a) Total alkali content (Na$_2$O + K$_2$O) versus SiO$_2$ for Wudi lavas compared to late Cenozoic basalts from eastern China (the literature data collected from the GEOROC database using the precompiled files made available at http://georoc.mpch-mainz.gwdg.de/georoc/ [see Table S5]). (b) Trace element patterns for clinopyroxene, and calculated melts in equilibrium with clinopyroxene and their host lavas from Wudi. The partition coefficients selected for calculating the compositions of the hypothetical liquids in equilibrium with clinopyroxenes are taken from experimental data (Hart & Dunn, 1993; Hauri et al., 1994). Data sources: carbonatite (Weiss et al., 2016), N-MORB (Workman & Hart, 2005), EM-1 lavas (Willbold & Stracke, 2006), and primitive mantle (McDonough & Sun, 1995). (c) Fo versus Ni content for olivine from Wudi lavas (Fo = 100 Mg/ (Mg + Fe), where Mg and Fe represent molar proportions). Literature data for olivine in low-silica basalts from Shandong Province are from Li et al. (2016) and Zhang et al. (2017). Olivine phenocrysts from MORB, komatiite, Hawaii, and HIMU (Mangaia and Tubuai) lavas are based on the data from Sobolev et al. (2007) and Weiss et al. (2016). The black bold curve is the calculated Ni content in olivine crystallized from all primary melts generated from a peridotite source with 1,960 ppm. Ni with the gray field representing ±1σ uncertainty (Herzberg et al., 2014); the black hatched area and black curves denote the calculated Ni content of olivine from olivine fractionated derivative melts from primary magmas (Herzberg et al., 2014). The blue and green lines are for olivine that crystallized from primary magmas (red crosses) generated from Ni-rich fertile peridotite with 2,360 ppm Ni that subsequently fractionated olivine and clinopyroxene (30% and 70%), and olivine, respectively (Herzberg et al., 2014).

Craton, near the Tan-Lu fault (Figure 1), occurs in the form of a small, isolated volcanic cone, covering 0.39 km^2 (Sakuyama et al., 2013; Zeng et al., 2010; Zhang et al., 2017). Samples for this study were collected from Wudi (Figure 1), and most of these samples are fresh without obvious alteration. The volcanic rocks are typically porphyritic with olivine and clinopyroxene phenocrysts (Figure S2 in the supporting information).

3. Methods

The analytical procedures for determining major and trace element concentrations and isotope ratios and quantitative Pb isotope evolution modeling are described in detail in the supporting information.

4. Results

Most Wudi lavas are classified as basanites and nephelinites on the total alkali-silica diagram (Figure 2a), exhibiting low SiO$_2$ (40.10–40.94 wt.%), and high total akali (6.60–7.30 wt.%) (Figure 2a), MgO (10.16–11.65 wt. %), and CaO (10.16–12.46 wt.%) contents (Figures S3a and S3b). In particular, among the late Cenozoic lavas in eastern China, the Wudi and Qixia lavas are the most depleted in SiO$_2$ (<42 wt.%) (Sakuyama et al., 2013; Zeng et al., 2010; Zhang et al., 2017) (Figures 2a and S3). Similar to other late Cenozoic lavas in eastern China, the Wudi lavas show oceanic island basalt (OIB)-like trace element patterns with enrichment in Nb and Ta but depletion in K, Pb, and Ti (Figure 2b). Notably, the Wudi lavas generally have higher incompatible element contents (Figure 2b) and Ce/Pb and Sm/Yb ratios (Figure S3b) compared to other lavas in eastern China. The Wudi lavas plot close to the depleted end of the array of the late Cenozoic lavas from eastern China on a ^{87}Sr/^{86}Sr versus ^{143}Nd/^{144}Nd diagram (Figure S4).

Two populations of olivine can be recognized in the Wudi basalts based on compositional features. A few olivines in the Wudi lavas have relatively low CaO and high Fo contents, similar to those from mantle xenoliths trapped by Mesozoic and Cenozoic volcanic rocks (see Figure S5). Most of the olivines show a large variation in Fo content (77.6 to 88) and has high CaO contents (>0.12 wt.%) (Figure S5). These olivines have higher CaO contents than those from mantle xenoliths (see Figure S5).

The major and trace element and Pb isotopes were measured in clinopyroxenes from six lava flows (see Tables S2 and S3). Clinopyroxenes in the Wudi basalts show large variation in Mg# (72.4–91.8) and Na$_2$O/TiO$_2$ (0.41–3.62) (Figure S6a). As shown in Figure S6d, clinopyroxene in the Wudi lavas can be divided into three groups. The first group consists of only a few clinopyroxenes, which are near to being in equilibrium with the Mg# of the whole rocks. The second group has low Mg# and plots below the equilibrium field, while a third group has high Mg# and plots above the equilibrium field (Figure S6d). Perhaps the most striking observation is that the Pb isotope compositions of the clinopyroxenes in the Wudi basalts vary markedly, exhibiting greater variation than the entire whole rock for the late Cenozoic lavas from eastern China (Figure 3). The Pb isotope values of clinopyroxenes from the Wudi basalts extend from the highly radiogenic HIMU field to that defined by the clinopyroxenes in mantle xenoliths from Cenozoic lavas (Figure 3).
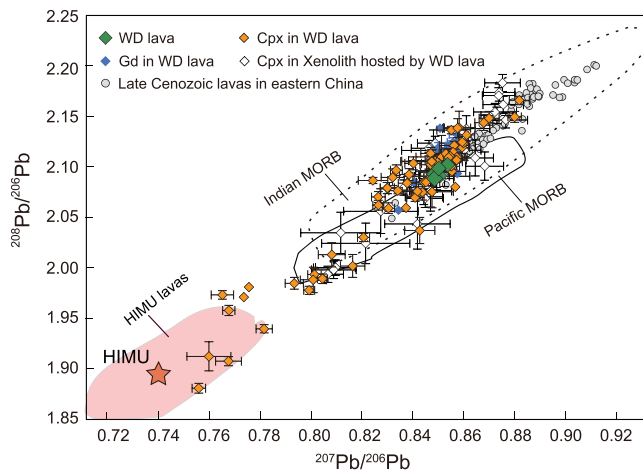
Figure 3. $^{207}Pb/^{206}Pb$ versus $^{208}Pb/^{206}Pb$ for whole rocks, groundmass (Gd) and clinopyroxene (Cpx) crystals from the Wudi lavas and Cpx in xenolith from Cenozoic lavas in eastern China. Data sources: late Cenozoic basalts in eastern China, typical HIMU lavas, and Pacific and Indian MORB are from the GEOROC database (http://georoc.mpchmainz.gwdg.de/georoc); DM and HIMU end-members are from Stracke et al. (2003). The error bars correspond to 2 standard error (2 SE).

5. Discussion

5.1. First Identification of the HIMU Component in the Mantle Source of Late Cenozoic Lavas From Eastern China

Given the resilience of clinopyroxene to postmagmatic alteration and the likelihood that the isotopic composition of fresh clinopyroxenes provides a faithful record of primary magmatic compositions (Hanyu & Nakamura, 2000; Jackson et al., 2009), the lack of isotopic equilibria between clinopyroxenes in the Wudi lavas provides strong evidence that some processes other than postmagmatic alteration has contributed to the observed isotopic disequilibrium.

The clinopyroxene in Wudi lavas are likely xenocrystic or magmatic origin. A few of the clinopyroxenes are similar in composition to those in mantle xenoliths, for example, showing low Sm/Yb and high Na/Ti and $^{207}Pb/^{206}Pb$ (see Figure S6), and thus are likely trapped by lavas during magma ascent. However, most clinopyroxene crystals in the Wudi basalts have much lower Mg# and Na_2O/TiO_2 and higher Sm/Yb than clinopyroxenes from mantle xenoliths in eastern China late Cenozoic basalts and oceanic basalts (Figures S6a–S6c). The compositional trend formed by clinopyroxenes in crustal xenoliths, such as granulites recovered from eastern China, is also distinct from most clinopyroxenes examined in this study (Figure S6a). The major and trace element and Pb isotopic data indicate that these clinopyroxenes are not xenocrysts entrained from the lithosphere during magma ascent and thus the lithosphere can be ruled out as a source of the nonequilibrium clinopyroxene.

As some clinopyroxenes in the Wudi basalts are in Pb isotopic disequilibrium with their groundmass and whole rocks (Figure 3), these clinopyroxenes clearly did not crystallize from liquids represented by their host groundmass or rock. The magmatic clinopyroxenes with relatively high Mg# also have high Na/Ti (Figure S6a), indicating that they crystallized at higher pressure and greater depth than other clinopyroxenes with relatively low Mg# and/or that they crystallized from unmixed parental magmas. These clinopyroxenes probably crystallized early as phenocrysts from hotter, higher-MgO (more primitive) melts (e.g., clinopyroxene with Mg# ranging from 89 to 90.2, which would be in equilibrium with melts with Mg# values of 69–71, Figure S6d). These magmatic clinopyroxenes record greater geochemical variability than host lavas and groundmass (Figures 3 and S6). This is consistent with the interpretation that the minerals crystallized from heterogeneous melts and probably preserve information on the chemical and isotopic diversity of unmixed melts, whereas the lavas are formed from mixtures of these melts and minerals (Davidson et al., 2007; Jackson et al., 2009; Sobolev et al., 2011). Furthermore, some Pb isotopic heterogeneity occurs on the millimeters scale, with differences in Pb isotopes between clinopyroxene cores and rims (Figures S6e and S6f). This can be interpreted to be due to multiple flows in the crystal mush leading to the juxtaposition of diverse populations of crystals (Hanyu & Nakamura, 2000; Jackson et al., 2009).

Some clinopyroxenes in the Wudi basalts have significantly lower $^{207}Pb/^{206}Pb$ ratios than late Cenozoic lavas in eastern China (Figure 3; note that the lowest $^{207}Pb/^{206}Pb$ ratios correspond to the most radiogenic Pb), while others have Pb isotope compositions similar to those in lithosphere beneath eastern China (Figure 3). The Pb isotope data for the clinopyroxenes from the Wudi basalts form quasi-linear arrays that can be largely explained by simple mixing of two end-members: one component rich in radiogenic Pb and identical to HIMU and the second component with a less radiogenic Pb composition represented by depleted lithosphere xenoliths in the lavas (Figure 3). Our findings document, for the first time, the presence of a HIMU-like mantle component in late Cenozoic lavas from eastern China. It is apparent from the Pb isotope data that shallow-level storage (e.g., melt-lithosphere interaction) and mixing of distinct magma batches resulted in homogenization and dilution of the radiogenic component within the Wudi magmas prior to eruption. Likewise, heterogeneous Pb isotopes recorded in melt inclusions from Hawaii, Iceland, and Mangaia lavas suggest that similar mixing processes of isotopically distinct parental magmas operate in shallow magma plumbing systems elsewhere (Maclennan, 2008; Saal et al., 1998; Sobolev et al., 2011). Minerals

(e.g., clinopyroxene) or melt inclusions likely provide important information on magmatic diversity that is invisible in the erupted lavas (Saal et al., 1998; Sobolev et al., 2011).

### 5.2. Nature and Origin of the HIMU End-Member Component

In general, the Wudi basalts have higher trace element contents and Ce/Pb, Sm/Yb, and Zr/Hf than depleted asthenospheric mantle (depleted mid-ocean ridge basalt mantle) and EM-1 lavas (Figures 2b and S7). Thus, the source must include a component with high Ce/Pb, Sm/Yb, and Zr/Hf. In terms of Sr-Nd isotope compositions, the Wudi basalts show a clear affinity with the HIMU end-member (Figure S4). However, the Wudi basalts do not have extremely high $^{206}Pb/^{204}Pb$ as would be expected for typical HIMU end-member (Figure S4). Interestingly, as indicated by Pb isotope compositions of the clinopyroxenes, a HIMU-like component is required to produce the Wudi basalts (Figure 3). Thus, partial melting of this HIMU-like component with high Ce/Pb, Sm/Yb, and Zr/Hf in the mantle source can explain the geochemical characteristics of the Wudi lavas in eastern China.

The HIMU end-member component is generally interpreted to represent subducted/recycled oceanic crust that has preferentially lost fluid-mobile trace elements during hydrothermal alteration or subduction (Hanyu et al., 2014; Lassiter & Hauri, 1998; Zindler & Hart, 1986), recycled mantle metasomatized by subduction-related carbonated oceanic crust (Homrighausen et al., 2018; Weiss et al., 2016), or recycled marine carbonates (Castillo, 2015). Interestingly, melts from dehydrated carbonate-bearing oceanic crust are characterized by high Ce/Pb, Zr/Hf, and Sm/Yb (Figure S7). Thus, melting dehydrated carbonate-bearing oceanic crust can account for the geochemical characteristics described above for the Wudi low-silica basalts (Figures S3 and S7). Additional evidence supporting the presence of a carbonate-bearing oceanic crust in the mantle source of the Wudi low-silica basalts arises from our new in situ trace element data for the clinopyroxenes. Notably, the trace element patterns of the liquid in equilibrium with the clinopyroxenes that have a HIMU signature, such as the depletion in fluid-mobile elements Ti, Zr and Hf, and enrichment in Nb and Ta, show striking similarities to carbonatites (Figure 2b). As characteristics of some magmatic clinopyroxene resemble those of carbonatites (e.g., superchondritic Zr/Hf ratios and high Ce/Pb), a carbonated mantle source may be involved during magma generation (Figure S7). The potential role of a CO_2-bearing component in the genesis of the low-silica basalts is also supported by the similarity between calculated parental melts compositions for low-silica basalts and melts produced experimentally from a CO_2-bearing source component (Figure S8). The injection of the carbonated Si-poor silicate melts derived from carbonated oceanic crust into normal mantle peridotite will produce carbonated peridotite, and olivine would not be converted to pyroxene and the lithology would be preserved (Weiss et al., 2016). Furthermore, the compositional variation in Ni contents of olivines from the low-silica basalts in eastern China is similar to that of olivines from other HIMU lavas worldwide, clearly pointing to a peridotite-dominated source (Figure 2c). Previously reported large-scale Mg-Zn isotope anomalies in late Cenozoic lavas further indicate the widespread presence of carbonated mantle beneath eastern China (Li et al., 2017).

Recent hypotheses suggest that HIMU signature is often associated with carbonatite-metasomatized mantle (Castillo, 2015; Homrighausen et al., 2018; Weiss et al., 2016). Globally, ocean island basalts trending toward the typical HIMU mantle are the most silica-undersaturated, and carbonate "globules" are found in Mangaia melt inclusions with HIMU signature (Saal et al., 1998), indicating a connection between HIMU signatures and carbonatite metasomatism. Carbonatitic melts proposed as a possible metasomatizing agent in mantle source, thus, could be the missing link in the generation of HIMU signature (Castillo, 2015; Weiss et al., 2016).

5.3. The Possible Genetic Model for the HIMU Mantle Source

Pb isotopes in the typical HIMU mantle source are too radiogenic to originate from an undifferentiated mantle or from depleted upper-mantle peridotite (Castillo, 2015). Our results do not support the formation of HIMU signature through recycling of dehydrated ocean crust, and instead the dominant source lithology is carbonated peridotite rather than eclogite/pyroxenite as the dominant source lithologies (Mazza et al., 2019; Weiss et al., 2016; Figures 2 and S8). The mantle source metasomatized by carbonatitic liquid has much higher μ values than the typical dehydrated ocean crust (Mazza et al., 2019). A Monte Carlo simulation (see section S1 for details in the supporting information and in Figure S9), similar to that of Mazza et al. (2019), is used to constrain the possible combinations of source age t and μ values that reproduce
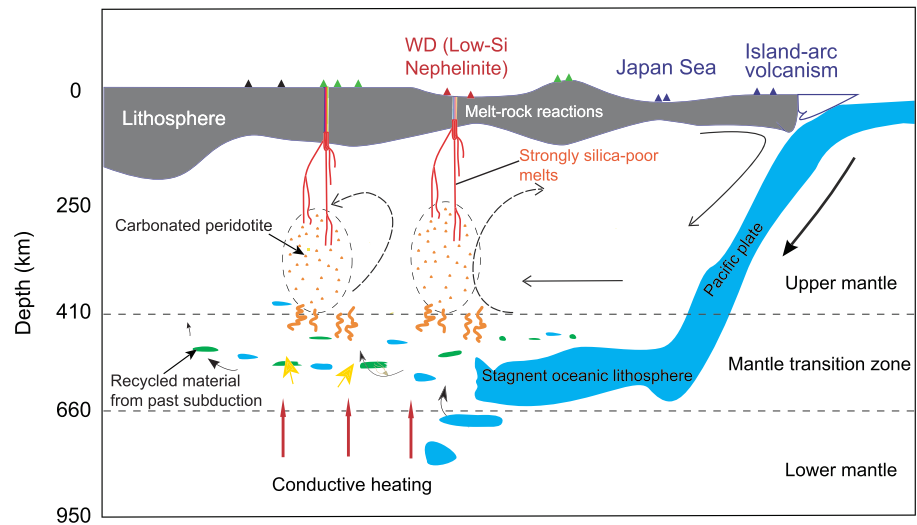
Figure 4. Schematic model to explain the late Cenozoic volcanism in eastern China as a product of small convection in the upper mantle. Mantle flow induced by slab subduction samples both the volatile-rich peridotite and the depleted upper mantle. Recycled material at the transition zone represents trapped subducted crust from previous subduction events.

the HIMU isotopic compositions. As shown in Figures S9 and S10, a high source μ value is required to generate the unique Pb composition of HIMU if the initial isotope value was similar to that of the least radiogenic sample of Paleo-Asian ocean crust; this is similar to the measured value (average $\mu = 40.8$) in the Wudi basalts (Figure S9). Our modeling suggests that the source age could be younger than 700 Ma with a minimum of $\mu > 34.9$ (Figure S9). This result implies that the Wudi silica-undersaturated basalts may sample a relatively young mantle domain, with extreme μ values, beneath eastern China.

Two potential regions within Earth where recycled materials are isolated are the base of the lower mantle (e.g., Weiss et al., 2016) or the MTZ (e.g., Kuritani et al., 2011; Mazza et al., 2019; Wang et al., 2017). However, both geophysical and geochemical evidence argue against a deep-rooted mantle plume beneath eastern China (Huang & Zhao, 2006; Wang et al., 2015). Thus, the metasomatically produced HIMU reservoir was possibly derived from the recycling and storage of carbonated material in the MTZ (Figure 4). On the basis of its unique geochemical characteristics, we suggest that the possible HIMU component is carbonatite-metasomatized materials formed in the last 700 Ma, from which we infer that it may be related to the subduction event of Paleo-Asian ocean that existed between 1 Ga and 300 Ma (Xiao et al., 2003). In this case, carbon- and water-rich liquids from subducted Paleo-Asian oceanic crust near the MTZ interacted with the ambient upper mantle (Castillo, 2015; Mazza et al., 2019), possibly in the presence of a K-hollandite mineral phase (Grassi et al., 2012). Experimental data suggest that at transition zone depths K, Pb, Rb, and Ba are favorably incorporated into K-hollandite during carbonatitic melt extraction, while Th, U, Nb, Ta, and rare earth elements (REEs) are preferentially partitioned into the carbonatitic melt (Grassi et al., 2012). This strong fractionation of certain elements in the mantle source imparted by carbonatitic liquid-related metasomatism can establish the observed time-integrated radiogenic isotope ratios of HIMU OIBs, notably the Pb isotope systematics, over much shorter timescales than billions of years (e.g., Halliday et al., 1995; Mazza et al., 2019). Furthermore, diamond inclusions provide evidence of the volatile-rich materials that can be stored in the MTZ (Walter et al., 2008). Our results provide further evidence that the isolation of recycled materials in the MTZ might be more important in the generation of mantle heterogeneities than previously thought. Thus, deep storage and recycling over billions of years may not be the only way in which extreme isotopic domains develop in the mantle (Mazza et al., 2019).

Two-dimensional geodynamic numerical models suggest that the volatile-rich top layer of the MTZ was sampled by disturbances related to mantle flow induced by dehydration of a stagnant slab (Sheng et al., 2016). Furthermore, sublithospheric small-scale convection readily entrains the volatile-rich materials near the base of the lithosphere, resulting in mantle melting and intraplate volcanism (Figure 4). We suggest that

the late Cenozoic lavas in eastern China started life as silica-poor melts from carbonated peridotite (Figure 4). These were in disequilibrium with the lithosphere and as a consequence reacted with it (Lundstrom, 2000). It is apparent from the geochemical data of the clinopyroxenes and lavas presented in this study that the silica-poor melts with HIMU-like signatures were readily diluted and "lost" in whole rocks as a result of shallow-level melt-lithosphere interaction and mixing of distinct magma batches (Figure 4). This is the possible reason for the rare occurrence of eruptions of HIMU lavas on the Earth's surface (e.g., on the islands of St Helena in the Atlantic Ocean, and Mangaia, Tubaii, and Rurutu in the Pacific Ocean) (Jackson et al., 2018).

6. Conclusions

In this study, we present new major and trace element, Sr-Nd-Pb isotope data for the Wudi basalts, and in situ Pb isotope data from clinopyroxenes and the groundmass in the same samples. The Wudi basalts are depleted in SiO_2 and enriched in FeOt. The Pb isotope compositions of clinopyroxenes in the Wudi basalts exhibit greater variation than the entire data set for late Cenozoic lavas from eastern China and form a linear array between the HIMU and depleted mantle components. This study documents, for the first time, a contribution from a HIMU-like component in the sources of late Cenozoic lava in eastern China. Our new data imply that the contribution from HIMU component in the formation of intraplate lavas may be more common than previously thought, despite the rarity of "pure" HIMU lavas at the Earth's surface. We argue that the storage of recycled materials in the MTZ is key to the production of extreme isotopic domains.

References

Castillo, P. R. (2015). The recycling of marine carbonates and sources of HIMU and FOZO ocean island basalts. *Lithos*, *216-217*, 254–263. https://doi.org/10.1016/j.lithos.2014.12.005

Chen, H., Xia, Q.-K., Ingrin, J., Deloule, E., & Bi, Y. (2017). Heterogeneous source components of intraplate basalts from NE China induced by the ongoing Pacific slab subduction. *Earth and Planetary Science Letters*, *459*, 208–220. https://doi.org/10.1016/j.epsl.2016.11.030

Chen, L. H., Zeng, G., Jiang, S. Y., Hofmann, A. W., Xu, X. S., & Pan, M. B. (2009). Sources of Anfengshan basalts: Subducted lower crust in the Sulu UHP belt, China. *Earth and Planetary Science Letters*, *286*(3–4), 426–435. https://doi.org/10.1016/j.epsl.2009.07.006

Davidson, J. P., Morgan, D. J., Charlier, B. L. A., Harlou, R., & Hora, J. M. (2007). Microsampling and isotopic analysis of igneous rocks: Implications for the study of magmatic systems. *Annual Review of Earth and Planetary Sciences*, *35*, 273–311. https://doi.org/10.1146/annurev.earth.35.031306.140211

Grassi, D., Schmidt, M. W., & Gunther, D. (2012). Element partitioning during carbonated pelite melting at 8, 13 and 22 GPa and the sediment signature in the EM mantle components. *Earth and Planetary Sciences*, *327*, 84–96. https://doi.org/10.1016/j.epsl.2012.01.023

Halliday, A. N., Lee, D.-C., Tommasini, S., Davies, G. R., Paslick, C. R., Godfrey Fitton, J., & James, D. E. (1995). Incompatible trace elements in OIB and MORB and source enrichment in the sub-oceanic mantle. *Earth and Planetary Sciences*, *133*(3), 379–395. https://doi.org/10.1016/0012-821X(95)00097-V

Hanyu, T., Kawabata, H., Tatsumi, Y., Kimura, J. I., Hyodo, H., Sato, K., et al. (2014). Isotope evolution in the HIMU reservoir beneath St. Helena: Implications for the mantle recycling of U and Th. *Geochimica Et Cosmochimica Acta*, *143*, 232–252. https://doi.org/10.1016/j.gca.2014.03.016

Hanyu, T., & Nakamura, E. (2000). Constraints on HIMU and EM by Sr and Nd isotopes re-examined. *Earth Planets and Space*, *52*(1), 61–70. https://doi.org/10.1186/BF03351614

Hart, S. R., & Dunn, T. (1993). Experimental cpx/melt partitioning of 24 trace elements. *Contributions to Mineralogy and Petrology*, *113*(1), 1–8. https://doi.org/10.1007/BF00320827

Hauri, E. H., Wagner, T. P., & Grove, T. L. (1994). Experimental and natural partitioning of Th, U, Pb and other trace elements between garnet, clinopyroxene and basaltic melts. *Chemical Geology*, *117*, 149–166. https://doi.org/10.1016/0009-2541(94)90126-0

Herzberg, C., Cabral, R. A., Jackson, M. G., Vidito, C., Day, J. M. D., & Hauri, E. H. (2014). Phantom Archean crust in Mangaia hotspot lavas and the meaning of heterogeneous mantle. *Earth and Planetary Science Letters*, *396*, 97–106. https://doi.org/10.1016/j.epsl.2014.03.065

Homrighausen, S., Hoernle, K., Hauff, F., Geldmacher, J., Wartho, J.-A., van den Bogaard, P., & Garbe-Schönberg, D. (2018). Global distribution of the HIMU end member: Formation through Archean plume-lid tectonics. *Earth-Science Reviews*, *182*, 85–101. https://doi.org/10.1016/j.earscirev.2018.04.009

Huang, J. L., & Zhao, D. P. (2006). High-resolution mantle tomography of China and surrounding regions. *Journal of Geophysical Research*, *111*, B09305. https://doi.org/10.1029/2005JB004066

Jackson, M. G., Becker, T. W., & Konter, J. G. (2018). Evidence for a deep mantle source for EM and HIMU domains from integrated geochemical and geophysical constraints. *Earth and Planetary Science Letters*, *484*, 154–167. https://doi.org/10.1016/j.epsl.2017.11.052

Jackson, M. G., Hart, S. R., Shimizu, N., & Blusztajn, J. S. (2009). The $^{87}Sr/^{86}Sr$ and $^{143}Nd/^{144}Nd$ disequilibrium between Polynesian hot spot lavas and the clinopyroxenes they host: Evidence complementing isotopic disequilibrium in melt inclusions. *Geochemistry, Geophysics, Geosystems*, *10*, Q03006. https://doi.org/10.1029/2008GC002324

Kimura, J.-I., Sakuyama, T., Miyazaki, T., Vaglarov, B. S., Fukao, Y., & Stern, R. J. (2018). Plume-stagnant slab-lithosphere interactions: Origin of the late Cenozoic intra-plate basalts on the East Eurasia margin. *Lithos*, *300–301*, 227–249. https://doi.org/10.1016/j.lithos.2017.12.003

Kuritani, T., Ohtani, E., & Kimura, J.-I. (2011). Intensive hydration of the mantle transition zone beneath China caused by ancient slab stagnation. *Nature Geoscience*, *4*(10), 713–716. https://doi.org/10.1038/ngeo1250

Lassiter, J. C., & Hauri, E. H. (1998). Osmium-isotope variations in Hawaiian lavas: Evidence for recycled oceanic lithosphere in the Hawaiian plume. *Earth and Planetary Science Letters*, *164*(3–4), 483–496. https://doi.org/10.1016/S0012-821x(98)00240-4

Li, S., Yang, W., Ke, S., Meng, X., Tian, H., Xu, L., et al. (2017). Deep carbon cycles constrained by a large-scale mantle Mg isotope anomaly in eastern China. *National Science Review*, *4*(1), 111–120. https://doi.org/10.1093/nsr/nww070

Li, H. Y., Xu, Y. G., Ryan, J. G., Huang, X. L., Ren, Z. Y., Guo, H., & Ning, Z. G. (2016). Olivine and melt inclusion chemical constraints on thesource of intracontinental basalts from the eastern North China Craton: Discrimination of contributions from the subducted Pacific slab. *Geochimica Et Cosmochimica Acta*, *178*, 1–19. https://doi.org/10.1016/j.gca.2015.12.032

Lundstrom, C. C. (2000). Rapid diffusive infiltration of sodium into partially molten peridotite. *Nature*, *403*(6769), 527–530. https://doi.org/10.1038/35000546

Maclennan, J. (2008). Lead isotope variability in olivine-hosted melt inclusions from Iceland. *Geochimica et Cosmochimica Acta*, *72*(16), 4159–4176. https://doi.org/10.1016/j.gca.2008.05.034

Mazza, S. E., Gazel, E., Bizimis, M., Moucha, R., Béguelin, P., Johnson, E. A., et al. (2019). Sampling the volatile-rich transition zone beneath Bermuda. *Nature*, *569*(7756), 398. https://doi.org/10.1038/s41586-019-1183-6

McCoy-West, A. J., Bennett, V. C., & Amelin, Y. (2016). Rapid Cenozoic ingrowth of isotopic signatures simulating "HIMU" in ancient lithospheric mantle: Distinguishing source from process. *Geochimica et Cosmochimica Acta*, *187*, 79–101. https://doi.org/10.1016/j.gca.2016.05.013

Mcdonough, W. F., & Sun, S. S. (1995). The Composition of the Earth. *Chemical Geology*, *120*(3-4), 223–253. https://doi.org/10.1016/0009-2541(94)00140-4

Saal, A. E., Hart, S. R., Shimizu, N., Hauri, E. H., & Layne, G. D. (1998). Pb isotopic variability in melt inclusions from oceanic island basalts, Polynesia. *Science*, *282*(5393), 1481–1484. https://doi.org/10.1126/science.282.5393.1481

Sakuyama, T., Tian, W., Kimura, J. I., Fukao, Y., Hirahara, Y., Takahashi, T., et al. (2013). Melting of dehydrated oceanic crust from the stagnant slab and of the hydrated mantle transition zone: Constraints from Cenozoic alkaline basalts in eastern China. *Chemical Geology*, *359*, 32–48. https://doi.org/10.1016/j.chemgeo.2013.09.012

Scott, J. M., Brenna, M., Crase, J. A., Waight, T. E., van der Meer, Q. H. A., Cooper, A. F., et al. (2016). Peridotitic lithosphere metasomatized by volatile-bearing melts, and its association with intraplate alkaline HIMU-like magmatism. *Journal of Petrology*, *57*(10), 2053–2078. https://doi.org/10.1093/petrology/egw069

Sheng, J., Liao, J., & Gerya, T. (2016). Numerical modeling of deep oceanic slab dehydration: Implications for the possible origin of far field intra-continental volcanoes in northeastern China. *Journal of Asian Earth Science*, *117*, 328–336. https://doi.org/10.1016/j.jseaes.2015.12.022

Sobolev, A. V., Hofmann, A. W., Jochum, K. P., Kuzmin, D. V., & Stoll, B. (2011). A young source for the Hawaiian plume. *Nature*, *476*(7361), 434–437. https://doi.org/10.1038/nature10321

Sobolev, A. V., Hofmann, A. W., Kuzmin, D. V., Yaxley, G. M., Arndt, N. T., Chung, S. L., et al. (2007). The amount of recycled crust in sources of mantle-derived melts. *Science*, *316*(5823), 412–417. https://doi.org/10.1126/science.1138113

Stracke, A., Bizimis, M., & Salters, V. J. M. (2003). Recycling oceanic crust: Quantitative constraints. *Geochemistry Geophysics Geosystems*, *4*(3), 8003. https://doi.org/10.1029/2001gc000223

Tang, Y. J., Zhang, H. F., & Ying, J. F. (2006). Asthenosphere-lithospheric mantle interaction in an extensional regime: Implication from the geochemistry of Cenozoic basalts from Taihang Mountains, North China Craton. *Chemical Geology*, *233*(3–4), 309–327. https://doi.org/10.1016/j.chemgeo.2006.03.013

Walter, M. J., Bulanova, G. P., Armstrong, L. S., Keshav, S., Blundy, J. D., Gudfinnsson, G., et al. (2008). Primary carbonatite melt from deeply subducted oceanic crust. *Nature*, *454*(7204), 622–625. http://www.nature.com/nature/journal/v454/n7204/suppinfo/nature07132_S1.html, https://doi.org/10.1038/nature07132

Wang, X. C., Wilde, S. A., Li, Q. L., & Yang, Y. N. (2015). Continental flood basalts derived from the hydrous mantle transition zone. *Nature Communications*, *6*. https://doi.org/10.1038/ncomms8700

Wang, X. J., Chen, L. H., Hofmann, A. W., Mao, F. G., Liu, J. Q., Zhong, Y., et al. (2017). Mantle transition zone-derived EM1 component beneath NE China: Geochemical evidence from Cenozoic potassic basalts. *Earth and Planetary Science Letters*, *465*, 16–28. https://doi.org/10.1016/j.epsl.2017.02.028

Weiss, Y., Class, C., Goldstein, S. L., & Hanyu, T. (2016). Key new pieces of the HIMU puzzle from olivines and diamond inclusions. *Nature*, *537*(7622), 666. https://doi.org/10.1038/nature19113

Willbold, M., & Stracke, A. (2006). Trace element composition of mantle end-members: Implications for recycling of oceanic and upper and lower continental crust. *Geochemistry Geophysics Geosystems*, *7*, Q04004. https://doi.org/10.1029/2005gc001005

Workman, R. K., & Hart, S. R. (2005). Major and trace element composition of the depleted MORB mantle (DMM). *Earth and Planetary Science Letters*, *231*(1), 53–72. https://doi.org/10.1016/j.epsl.2004.12.005

Xiao, W., Windley, B. F., Hao, J., & Zhai, M. (2003). Accretion leading to collision and the Permian Solonker suture, Inner Mongolia, China: Termination of the central Asian orogenic belt. *Tectonics*, *22*(6). https://doi.org/10.1029/2002TC001484

Zeng, G., Chen, L. H., Xu, X. S., Jiang, S. Y., & Hofmann, A. W. (2010). Carbonated mantle sources for Cenozoic intra-plate alkaline basalts in Shandong, North China. *Chemical Geology*, *273*(1–2), 35–45. https://doi.org/10.1016/j.chemgeo.2010.02.009

Zhang, J. B., Liu, Y. S., Ling, W. L., & Gao, S. (2017). Pressure-dependent compatibility of iron in garnet: Insights into the origin of ferro-picritic melt. *Geochimica et Cosmochimica Acta*, *197*, 356–377. https://doi.org/10.1016/j.gca.2016.10.047

Zindler, A., & Hart, S. (1986). Chemical geodynamics. *Annual Review of Earth and Planetary Sciences*, *14*, 493–571. https://doi.org/10.1146/annurev.earth.14.1.493

References From the Supporting Information

Chu, Z. Y., Chen, F. K., Yang, Y. H., & Guo, J. H. (2009). Precise determination of Sm, Nd concentrations and Nd isotopic compositions at the nanogram level in geological samples by thermal ionization mass spectrometry. *Journal of Analytical Atomic Spectrometry*, *24*(11), 1534–1544. https://doi.org/10.1039/b904047a

Chu, Z. Y., Wu, F. Y., Walker, R. J., Rudnick, R. L., Pitcher, L., Puchtel, I. S., et al. (2009). Temporal evolution of the lithospheric mantle beneath the eastern North China Craton. *Journal of Petrology*, *50*, 1857–1898. https://doi.org/10.1093/petrology/egp055

Dasgupta, R., Jackson, M. G., & Lee, C.-T. A. (2010). Major element chemistry of ocean island basalts—Conditions of mantle melting and heterogeneity of mantle source. *Earth and Planetary Science Letters*, *289*(3), 377–392. https://doi.org/10.1016/j.epsl.2009.11.027

Elburg, M., Vroon, P., van der Wagt, B., & Tchalikian, A. (2005). Sr and Pb isotopic composition of five USGS glasses (BHVO-2G, BIR-1G, BCR-2G, TB-1G, NKT-1G). *Chemical Geology*, *223*(4), 196–207. https://doi.org/10.1016/j.chemgeo.2005.07.001

Gao, S., Rudnick, R. L., Xu, W., Yuan, H., Liu, Y., Walker, R. J., et al. (2008). Recycling deep cratonic lithosphere and generation of intraplate magmatism in the North China Craton. *Earth and Planetary Science Letters*, *270*(1–2), 41–53. https://doi.org/10.1016/j.epsl.2008.03.008

Liu, Y., Gao, S., Yuan, H., Zhou, L., Liu, X., Wang, X., et al. (2004). U-Pb zircon ages and Nd, Sr, and Pb isotopes of lower crustal xenoliths from North China Craton: Insights on evolution of lower continental crust. *Chemical Geology*, *211*(1–2), 87–109. https://doi.org/10.1016/j.chemgeo.2004.06.023

Liu, Y. S., Hu, Z. C., Gao, S., Günther, D., Xu, J., Gao, C. G., & Chen, H. H. (2008). In situ analysis of major and trace elements of anhydrous minerals by LA-ICP-MS without applying an internal standard. *Chemical Geology*, *257*(1–2), 34–43. https://doi.org/10.1016/j.chemgeo.2008.08.004

Mathez, E., & Waight, T. E. (2003). Lead isotopic disequilibrium between sulfide and plagioclase in the Bushveld complex and the chemical evolution of large layered intrusions. *Geochimica et Cosmochimica Acta*, *67*(10), 1875–1888.

Putirka, K. (1999). Clinopyroxeneþliquid equilibria to 100 kbar and 2450 K. *Contributions to Mineralogy and Petrology*, *135*, 151–163. https://doi.org/10.1007/s004100050503

Souders, A. K., & Sylvester, P. J. (2010). Accuracy and precision of non-matrix-matched calibration for lead isotope ratio measurements of lead-poor minerals by LA-MC-ICPMS. *Journal of Analytical Atomic Spectrometry*, *25*(7), 975–988.

Todt, W., Cliff, R. A., Hanser, A., & Hofmann, A. W. (1996). Evaluation of a ^{202}Pb–^{205}Pb double spike for high precision lead isotope analysis. In *Earth processes: Reading the isotopic code*, (pp. 429–437). Washington, DC: American Geophysical Union. https://doi.org/10.1029/GM095p0429

Wang, S. (2009). Geochemistry and implications of ophiolite in central Inner Mongolia. Master Thesis, Guangzhou Institute of Geochemistry, Chinese Academy of Sciences, Guangzhou, China, p. 75 (in Chinese with English abstract).

Wiedenbeck, M., Alle, P., Corfu, F., Griffin, W. L., Meier, M., Ober, F., et al. (1995). Three natural zircon standards for U-Th-Pb, Lu-Hf, trace element and REE analyses. *Geostandards and Geoanalytical Research*, *19*(1), 1–23. https://doi.org/10.1111/j.1751-908X.1995.tb00147.x

Xia, L., Li, X. M., Xu, X. Y., Xia, Z. C., Ma, Z. P., & Wang, L. S. (2005). Petrogenetic evolution of the Bayan Gol Ophiolit—Geological record of an early carboniferous "Red Sea type" ocean basin in the Tianshan Mountains, northwestern China. *Acta Geologica Sinica – English Ed*, *79*, 174–192.

Ying, J. F., Zhang, H. F., & Tang, Y. J. (2010). Lower crustal xenoliths from Junan, Shandong province and their bearing on the nature of the lower crust beneath the North China Craton. *Lithos*, *119*(3–4), 363–376. https://doi.org/10.1016/j.lithos.2010.07.015

Zhang, L., Ren, Z. Y., Nichols, A. R. L., Zhang, Y. H., Zhang, Y., Qian, S. P., & Liu, J. Q. (2014). Lead isotope analysis of melt inclusions by LA-MC-ICP-MS. *Journal of Analytical Atomic Spectrometry*, *29*(8), 1393–1405. https://doi.org/10.1039/c4ja00088a